24th INTERNATIONAL CONGRESS ON SOUND AND VIBRATION
23–27 July 2017, London

METAMATERIAL PANEL WITH ARRAYS OF PIEZOELECTRIC PATCHES CONNECTED TO MULTI-RESONANT ELECTRICAL SHUNTS

Michal Zientek, Paolo Gardonio

Università Degli Studi di Udine, DPIA, Via delle Scienze 206, Udine, Italy
email: michal.zientek@uniud.it

This paper presents a simulation study on the feasibility of a smart metamaterial panel designed to reduce the flexural vibrations in wide frequency ranges. The system is composed by a thin aluminium plate with a dense two dimensional array of shunted piezoelectric patch transducers. The plate is exposed to a rain on the roof time and spatial stochastic excitation. The overall flexural response of the plate is derived in terms of the time averaged total flexural kinetic energy. The piezoelectric patch transducers are connected to multi-resonating shunts specifically designed to suppress flexural vibration of the plate over multiple frequency bands. The overall vibration control effect is obtained both via the regular arrangement of the patches on the panel and via the multi-resonating shunts, which are optimized to maximise the absorbed electrical power over target frequency bands.
Keywords: acoustic metamaterial, piezoelectric patch, electric shunt, vibration absorber

1. Introduction

This work investigates the vibration control effects produced in a thin panel by a periodic array of piezoelectric patches connected to multi-resonant shunts that mimic multi-modal vibration absorbers. The vibration stop band effect in periodic structures has been the subject of many studies for a long time now and the structural wave interference phenomena that characterise this phenomenon are described in books, such as for example ref. [1]. More recently the vibration stop band effects produced on structures by regular arrays of resonating inclusions has also been investigated [2]. In this case, the stop band effect is due to both the structural wave interference effect produced by the regular spacing of the inclusions and by the interaction between the resonant response of the inclusions and the structural wave propagation in the structure. In this work, the effects produced on a thin panel by a periodic array of piezoelectric patch transducers connected to multi-resonant shunts set to maximise the absorbed electric power are investigated. The idea of using shunted piezoelectric patch transducers to reduce vibrations of mechanical systems and flexible structures was first proposed by Forward [3]. Since then, many studies were carried out on this topic [4-7], which considered a wide range of solutions, ranging from classical RL shunts to more complex circuits involving active elements that implement negative capacitance effects or multi-resonant electric networks. Recently, research work has also been focussed on the development of structures with dense arrays of shunted piezoelectric patches that mimic an array of resonators and thus produce stop band phenomena due to both structural wave interference and vibration absorption effects [8-11].

This work starts with the description of the panel system with a grid of multi-resonant shunted piezoelectric patches. The details of the mathematical model used to obtain the simulation results are then presented in section 3. The vibration control effects produced when the array of multi-resonant shunted piezoelectric patches is either set to minimise the time averaged total flexural kinetic energy of the panel, i.e. the overall flexural response of the panel, or it is tuned to maximise the time averaged total electric power absorbed by the shunts is analysed and contrasted in section 4.

2. Description of the system

Figure 1 shows the smart plate system considered in this study, which is composed by a simply supported rectangular thin plate, whose geometry and physical properties are summarized in Tab. 1. As depicted in Figure 1A, the plate is exposed to a white noise rain-on-the-roof excitation, which is modelled in terms of a 4×4=16 array of uncorrelated point forces uniformly distributed over the surface of the plate. An array of 9×7=63 patches is arranged on the plate as shown in Figure 1B. Each patch is connected to a multi-resonant shunt, which is composed by a cascade of parallel RLC meshes (Fig. 1C).

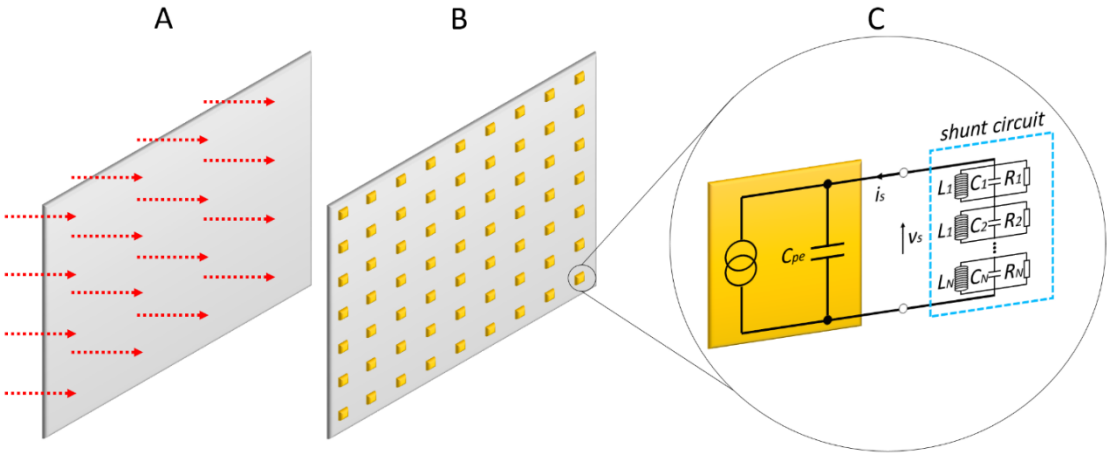

Figure 1: Plate subject to a rain on the roof excitation modelled as a 4×4 array of uncorrelated point forces (A) and equipped with an array of 9×7 piezoelectric patch transducers (B), connected to multi-resonant shunts (C).

Table 1: Dimensions and physical properties of the panel and piezoelectric patches.

	Plate	**Piezoelectric patches**
dimensions	$l_{xp} \times l_{yp} = 414 \times 314\ mm$	$l_{pe} \times l_{pe} = 11 \times 10\ mm$
Thickness	$h_p = 1\ mm$	$h_{pe} = 1\ mm$
Density	$\rho_p = 2700\ kg/m^3$	$\rho_{pe} = 7600\ kg/m^3$
Young's modulus	$E_p = 7 \times 10^{10}\ N/m^2$	$E_{pe} = 2.7 \times 10^{10}\ N/m^2$
Poisson ratio	$\upsilon_p = 0.33$	$\upsilon_{pe} = 0.275$
modal damping ratio	$\zeta_p = 0.02$	$l_{pe} \times l_{pe} = 1.1 \times 1\ mm$
periodicity length	$35\ mm$	
strain/charge constants		$d_{31}^0 = d_{32}^0 = 150 \times 10^{-12}\ m/V$
		$d_{36}^0 = 0$
permittivity		$\varepsilon_{pe} = 84 \times 10^{-9}\ F/m$
capacitance		$C_{pe} = 3.167 \times 10^{-9}\ F$

3. Mathematical model

3.1 Mechanical and electrical equations

The mathematical formulation for the coupled flexural response of the panel and piezoelectric patches is based on Refs. [12,13] and considers the classical theory of out of plane flexural vibrations in thin plates that refers to Kirchhoff hypothesis [14]. In-plane vibrations are not taken into account, which is a reasonable assumption within the considered frequency range (20 Hz – 1 kHz). The response of the system is derived from the generalized form of Hamilton's principle for electromechanical systems [14-17]. Two matrix equations are derived for the flexural response of the panel, which is expressed in terms of *R* modal coordinates for the flexural modes of the plain panel [18], and for the electric response of the shunts [12,13]:

$$\mathbf{M}_t\ddot{\mathbf{q}}(t) + \mathbf{C}_p\dot{\mathbf{q}}(t) + \mathbf{K}_t\mathbf{q}(t) + \boldsymbol{\theta}_{pe}\mathbf{v}_s(t) = \boldsymbol{\Phi}_p\mathbf{f}_p(t)\,, \tag{1}$$

$$-\boldsymbol{\theta}_{pe}^T\dot{\mathbf{q}}(t) + \mathbf{C}_{pe}\ddot{\boldsymbol{\lambda}}_s(t) = \mathbf{i}_s(t)\,. \tag{2}$$

Here $\mathbf{q} = \lfloor q_1 \quad \cdots \quad q_R \rfloor^T$ is the vector with the modal coordinates, $\mathbf{f}_\mathrm{p} = \lfloor f_{p1} \quad \cdots \quad f_{p16} \rfloor^T$ is the vector with the amplitudes of the 4×4 array of forces acting on the plate. As shown in Refs. [12,13], $\mathbf{M}_t = \mathbf{M}_p + \mathbf{M}_{pe}$ and $\mathbf{K}_t = \mathbf{K}_p + \mathbf{K}_{pe}$ are the R×R modal mass and stiffness matrices, which are given by the sum of a diagonal matrix for the plate effect and a fully populated matrix for the piezoelectric patches effects. Also, $\mathbf{C}_p$ is the R×R modal damping matrix of the plate and $\boldsymbol{\Phi}_p$ is a R×16 matrix with the modal amplitudes at the excitation points. The vectors $\boldsymbol{\lambda}_s = \lfloor \lambda_{s1} \quad \cdots \quad \lambda_{s63} \rfloor^T$ and $\mathbf{i}_s = \lfloor i_{s1} \quad \cdots \quad i_{s63} \rfloor^T$ contain the flux linkages and currents of the shunts (N.B. $\dot{\boldsymbol{\lambda}}_s = \mathbf{v}_s$ where $\mathbf{v}_s = \lfloor v_{s1} \quad \cdots \quad v_{s63} \rfloor^T$ is the vector with the shunts voltages). Also, the 63×63 diagonal matrix $\mathbf{C}_{pe}$ contains the capacitances of the piezoelectric patches $C_{pe} = \varepsilon_{pe}^S A_{pe}/h_{pe}$. Finally, $\boldsymbol{\theta}_{pe}$ is the R×63 piezoelectric coupling matrix. The details of all these matrices can be found in Refs. [12,13].

3.2 Multi-modal shunt electrical equations

As depicted in Figure 1C, each shunt is characterised by a cascade or parallel RLC meshes, which are assumed equal for all shunts. Assuming the electrical functions are time-harmonic and given in the form $f(\mathrm{t}) = f(\omega)\exp(\mathrm{j}\omega)$, where $f(\omega)$ is the complex amplitude, ω is the circular frequency and $\mathrm{j} = \sqrt{-1}$, the impedance of the cascade of parallel RLC meshes in each shunt circuit can be expressed with the following series of N second order terms:

$$\frac{v_{s,i}(\omega)}{i_{s,i}(\omega)} = \frac{\dot{\lambda}_{s,i}(\omega)}{i_{s,i}(\omega)} = -Z_{s,i}(\omega) = -\frac{\mathrm{j}\omega\left(\frac{1}{C_1}\right)}{-\omega^2+\mathrm{j}\omega\left(\frac{\omega_{n1}}{Q_1}\right)+\omega_{n1}^2} - \frac{\mathrm{j}\omega\left(\frac{1}{C_2}\right)}{-\omega^2+\mathrm{j}\omega\left(\frac{\omega_{n2}}{Q_2}\right)+\omega_{n2}^2} - \cdots - \frac{\mathrm{j}\omega\left(\frac{1}{C_N}\right)}{-\omega^2+\mathrm{j}\omega\left(\frac{\omega_{nN}}{Q_N}\right)+\omega_{nN}^2}\,, \tag{3}$$

where $\omega_{nj} = 1/\sqrt{L_{sj}C_{sj}}$ and $Q_j = R_{sj}\sqrt{C_{sj}/L_{sj}}$ are respectively the natural frequency and quality factor of the j-th RLC mesh characterised by inductance L_{sj}, capacitance C_{sj} and resistance R_{sj}. Each second order term in Eq. (3) can be envisaged as the ratio between a "modal" voltage $V_{s,j}$, i.e. flux linkage rate $\dot{\Lambda}_{s,j}$, and current $I_{s,j}$. Thus, the flux linkage can be expressed with the following matrix equation

$$\lambda_s(\omega) = -\boldsymbol{\Psi}_s\boldsymbol{\Lambda}_s(\omega), \tag{4}$$

where $\boldsymbol{\Psi}_s = \left[\frac{1}{\sqrt{C_s}} \ldots \frac{1}{\sqrt{C_s}}\right]$ and $\boldsymbol{\Lambda}_s(\omega) = \lfloor \Lambda_{s1} \quad \cdots \quad \Lambda_{sN} \rfloor^T$ is the vector with the modal flux linkages, which can expressed in terms of the modal currents by the following matrix relation

$$\boldsymbol{\Lambda}_s(\omega) = \mathbf{G}_s(\omega)\mathbf{I}_s(\omega)\,, \tag{5}$$

that is

$$\begin{bmatrix} \Lambda_{s1}(\omega) \\ \\ \\ \Lambda_{sN}(\omega) \end{bmatrix} = -\begin{bmatrix} \frac{1}{-\omega^2+\mathrm{j}\omega\left(\frac{\omega_{n1}}{Q_1}\right)+\omega_{n1}^2} & & \\ & \ddots & \\ & & \frac{1}{-\omega^2+\mathrm{j}\omega\left(\frac{\omega_{nN}}{Q_N}\right)+\omega_{nN}^2} \end{bmatrix} \begin{bmatrix} I_{s1}(\omega) \\ \\ \\ I_{sN}(\omega) \end{bmatrix}. \tag{6}$$

Here $\mathbf{I}_s(\omega) = \lfloor I_{s1} \quad \cdots \quad I_{sN} \rfloor^T$ is the vector with the modal flux linkages, which in turn is given by

$$\mathbf{I}_s(\omega) = \boldsymbol{\Psi}_s^T i_s(\omega)\,. \tag{7}$$

Considering the expanded form in Eq. (6), the frequency domain Eq. (5) can be straightforwardly transformed into the following time domain expression:

$$\boldsymbol{\Pi}_s\ddot{\boldsymbol{\Lambda}}_s(t) + \boldsymbol{\Delta}_s\dot{\boldsymbol{\Lambda}}_s(t) + \boldsymbol{\Omega}_s^2\boldsymbol{\Lambda}_s(t) = -\mathbf{I}_s(t)\,, \tag{8}$$

where

$$\mathbf{\Pi}_s = \begin{bmatrix} 1 & & \\ & \ddots & \\ & & 1 \end{bmatrix}, \quad \mathbf{\Delta}_s = \begin{bmatrix} \frac{\omega_{n1}}{Q_1} & & \\ & \ddots & \\ & & \frac{\omega_{nN}}{Q_N} \end{bmatrix}, \quad \mathbf{\Omega}_s = \begin{bmatrix} \omega_{n1} & & \\ & \ddots & \\ & & \omega_{nN} \end{bmatrix}. \tag{9-11}$$

Now, considering 63 independent shunt circuits, Eq. (8) becomes

$$\widehat{\mathbf{\Pi}}_s \ddot{\widehat{\mathbf{\Lambda}}}_s(t) + \widehat{\mathbf{\Delta}}_s \dot{\widehat{\mathbf{\Lambda}}}_s(t) + \widehat{\mathbf{\Omega}}_s^2 \widehat{\mathbf{\Lambda}}_s(t) = -\hat{\mathbf{I}}_s(t) \,, \tag{12}$$

where $\widehat{\mathbf{\Lambda}}_s = [\mathbf{\Lambda}_{s1}^T \quad \cdots \quad \mathbf{\Lambda}_{s63}^T]^T$, $\hat{\mathbf{I}}_s = [\mathbf{I}_{s1}^T \quad \cdots \quad \mathbf{I}_{s63}^T]^T$, and

$$\widehat{\mathbf{\Pi}}_s = \begin{bmatrix} \mathbf{\Pi}_{s1} & & \\ & \ddots & \\ & & \mathbf{\Pi}_{s63} \end{bmatrix}, \quad \widehat{\mathbf{\Delta}}_s = \begin{bmatrix} \mathbf{\Delta}_{s1} & & \\ & \ddots & \\ & & \mathbf{\Delta}_{s63} \end{bmatrix}, \quad \widehat{\mathbf{\Omega}}_s = \begin{bmatrix} \mathbf{\Omega}_{s1} & & \\ & \ddots & \\ & & \mathbf{\Omega}_{s63} \end{bmatrix}. \tag{13-15}$$

Also Eqs. (4) and (7) become

$$\boldsymbol{\lambda}_s(\omega) = -\widehat{\mathbf{\Psi}}_s \widehat{\mathbf{\Lambda}}_s(\omega), \quad \hat{\mathbf{I}}_s(\omega) = \widehat{\mathbf{\Psi}}_s^T \mathbf{i}_s(\omega) \,, \tag{16,17}$$

where the rectangular matrix $\widehat{\mathbf{\Psi}}_s$ is assembled as follows:

$$\widehat{\mathbf{\Psi}}_s = \begin{bmatrix} \mathbf{\Psi}_{s1}^T & & \\ & \ddots & \\ & & \mathbf{\Psi}_{sN}^T \end{bmatrix}. \tag{18}$$

3.3 Filtered response of the output modal velocities and shunt currents

The multi-resonant shunts have been tuned in such a way as to either minimise the time averaged total flexural response of the panel or to maximise the time averaged total electrical power absorbed by the shunts filtered within a series of adjacent frequency bands. Thus, the conversion to filtered modal coordinates and filtered shunt magnetic flux linkages is derived here. For convenience, simple, second order filters were implemented such that:

$$\mathbf{q}_f(\omega) = \boldsymbol{G}_{\mathrm{q}}(\omega)\mathbf{q}(\omega) \quad \text{and} \quad \widehat{\mathbf{\Lambda}}_{sf}(\omega) = \boldsymbol{G}_{\Lambda}(\omega)\widehat{\mathbf{\Lambda}}_s(\omega) \,, \tag{19,20}$$

where $\boldsymbol{G}_{\mathrm{q}}$ and $\boldsymbol{G}_{\Lambda}$ are diagonal matrices whose elements for the *k*-th filtering band are all equal to:

$$G_{f,k}(\omega) = \frac{\mathrm{j}\omega(\omega_k/Q_k)}{-\omega^2 + \mathrm{j}\omega(\omega_k/Q_k) + \omega_k^2} \,. \tag{21}$$

Here $\omega_k = \sqrt{\omega_{kmin}\omega_{kmax}}$ is the centre frequency and Q_k is the quality factor of the filters. As seen in the previous section, the frequency Eqs. (19), (20), can be straightforwardly casted into time domain equations, which take the following forms:

$$\mathbf{\Pi}_f \ddot{\mathbf{q}}_f(t) + \mathbf{\Delta}_f \dot{\mathbf{q}}_f(t) + \mathbf{\Omega}_f^2 \mathbf{q}_f(t) = \dot{\mathbf{q}}(t) \,, \quad \widehat{\mathbf{\Pi}}_f \ddot{\widehat{\mathbf{\Lambda}}}_f(t) + \widehat{\mathbf{\Delta}}_f \dot{\widehat{\mathbf{\Lambda}}}_f(t) + \widehat{\mathbf{\Omega}}_f^2 \widehat{\mathbf{\Lambda}}_f(t) = \dot{\widehat{\mathbf{\Lambda}}}(t) \,. \tag{22,23}$$

Considering the *k*-th filtering band, $\mathbf{\Pi}_f$ and $\widehat{\mathbf{\Pi}}_f$ are identity matrices, $\mathbf{\Delta}_f$ and $\widehat{\mathbf{\Delta}}_f$ are diagonal matrices with all terms equal to ω_k/Q_k and $\mathbf{\Omega}_f$ and $\widehat{\mathbf{\Omega}}_f$ are diagonal matrices with all terms equal to ω_k.

3.4 State Space Formulation

The time domain Eqs. (1), (2), (12), (22), (23) were employed to generate a State Space formulation for the response and filtered response of the system. First of all, Eq. (1) was rewritten as follows:

$$\ddot{\mathbf{q}}(t) = -\mathbf{M}_t^{-1}\mathbf{K}_t\mathbf{q}(t) - \mathbf{M}_t^{-1}\mathbf{C}_p\dot{\mathbf{q}}(t) - \mathbf{M}_t^{-1}\boldsymbol{\theta}_{pe}\mathbf{v}_s(t) + \mathbf{M}_t^{-1}\mathbf{\Phi}_p\mathbf{f}_p(t) \,. \tag{24}$$

Also, Eqs. (12), (16), (17) were used to rewrite the electric Eq. (2) in terms of the modal flux linkages. This was accomplished by pre-multiplying the left and right hand side of Eq. (2) by $\widehat{\boldsymbol{\theta}}_{pe}^T$ such that, using Eqs. (16) and (17), the following expression was obtained:

$$-\widehat{\boldsymbol{\Psi}}_s^T\boldsymbol{\theta}_{pe}^T\dot{\mathbf{q}}(t)+\widehat{\boldsymbol{\Psi}}_s^T\mathbf{C}_{pe}\ddot{\boldsymbol{\lambda}}_s(t)=-\widehat{\boldsymbol{\Psi}}_s^T\boldsymbol{\theta}_{pe}^T\dot{\mathbf{q}}(t)+\widehat{\boldsymbol{\Psi}}_s^T\mathbf{C}_{pe}\widehat{\boldsymbol{\Psi}}_s\ddot{\widehat{\boldsymbol{\Lambda}}}_s(t)=\widehat{\boldsymbol{\Psi}}_s^T\mathbf{i}_s(t)=\hat{\mathbf{I}}_s(t)\,. \tag{25}$$

Eq. (12) was then substituted in the right hand side of this equation such that:

$$\ddot{\widehat{\boldsymbol{\Lambda}}}_s(t)=\hat{\mathbf{C}}_{pe}^{-1}\widehat{\boldsymbol{\theta}}_{pe}^T\dot{\mathbf{q}}(t)-\hat{\mathbf{C}}_{pe}^{-1}\widehat{\boldsymbol{\Delta}}_s\dot{\widehat{\boldsymbol{\Lambda}}}_s(t)-\hat{\mathbf{C}}_{pe}^{-1}\widehat{\boldsymbol{\Omega}}_s^2\widehat{\boldsymbol{\Lambda}}_s(t)\,, \tag{26}$$

where $\hat{\mathbf{C}}_{pe}=\left[\hat{\mathbf{I}}+\widehat{\boldsymbol{\Psi}}_s^T\mathbf{C}_{pe}\widehat{\boldsymbol{\Psi}}_s\right]$ and $\widehat{\boldsymbol{\theta}}_{pe}^T=\widehat{\boldsymbol{\Psi}}_s^T\boldsymbol{\theta}_{pe}^T$. Finally, to work out the time-derivative term in the second member, Eqs. (22) and (23) were rewritten with respect to the following new vectors for the modal coordinates and modal flux linkages

$$\mathbf{q}_{f'}(t)=\dot{\mathbf{q}}_f(t)-\boldsymbol{\Delta}_f\mathbf{q}(t)\ \text{ and }\ \widehat{\boldsymbol{\Lambda}}_{sf'}(t)=\dot{\widehat{\boldsymbol{\Lambda}}}_{sf}(t)-\widehat{\boldsymbol{\Delta}}_{sf}\widehat{\boldsymbol{\Lambda}}_s(t) \tag{27,28}$$

such that, after some mathematical manipulations, they were transformed in the following matrix expressions:

$$\dot{\mathbf{q}}_{f'}(t)=-\boldsymbol{\Omega}_f\mathbf{q}_f(t)-\boldsymbol{\Delta}_f\mathbf{q}_{f'}(t)-\boldsymbol{\Delta}_f^2\mathbf{q}(t)\,,\ \dot{\widehat{\boldsymbol{\Lambda}}}_{sf'}(t)=-\widehat{\boldsymbol{\Omega}}_{sf}\widehat{\boldsymbol{\Lambda}}_{sf}(t)-\widehat{\boldsymbol{\Delta}}_{sf}\widehat{\boldsymbol{\Lambda}}_{sf'}(t)-\widehat{\boldsymbol{\Delta}}_{sf}^2\widehat{\boldsymbol{\Lambda}}_s(t)\,. \tag{29,30}$$

At this point, Eqs. (24), (26), (29) (30) were ready to be used to construct the state space formulation with respect to the state vector

$$\mathbf{x}(t)=\left[\mathbf{q}^T\quad\dot{\mathbf{q}}^T\quad\mathbf{q}_f^T\quad\mathbf{q}_{f'}^T\quad\widehat{\boldsymbol{\Lambda}}_s^T\quad\dot{\widehat{\boldsymbol{\Lambda}}}_s^T\quad\widehat{\boldsymbol{\Lambda}}_{sf}^T\quad\widehat{\boldsymbol{\Lambda}}_{sf'}^T\right]^T. \tag{31}$$

A classical state space formulation was thus derived with three output equations, one for the modal coordinates of the structural response, one for the filtered modal coordinates of the structural response and one for the filtered flux linkages of the shunts:

$$\dot{\mathbf{x}}(t)=\mathbf{A}\mathbf{x}(t)+\mathbf{B}\boldsymbol{f}_p(t), \tag{32}$$

$$\dot{\mathbf{q}}(t)=\mathbf{C}_{\mathbf{q}}\mathbf{x}(t)\,,\quad\dot{\mathbf{q}}_f(t)=\mathbf{C}_{\mathbf{q}f}\mathbf{x}(t)\,,\quad\dot{\widehat{\boldsymbol{\Lambda}}}_{sf}(t)=\mathbf{C}_{\boldsymbol{\Lambda}f}\mathbf{x}(t)\,. \tag{33-35}$$

The state space and the input/output matrices were derived as follows

$$\mathbf{A}=\begin{bmatrix}\mathbf{0}&\mathbf{I}&\mathbf{0}&\mathbf{0}&\mathbf{0}&\mathbf{0}&\mathbf{0}&\mathbf{0}\\-\mathbf{M}_t^{-1}\mathbf{K}_t&-\mathbf{M}_t^{-1}\mathbf{C}_p&\mathbf{0}&\mathbf{0}&-\mathbf{M}_t^{-1}\widehat{\boldsymbol{\theta}}_{pe}&\mathbf{0}&\mathbf{0}&\mathbf{0}\\\boldsymbol{\Delta}_f&\mathbf{0}&\mathbf{0}&\mathbf{I}&\mathbf{0}&\mathbf{0}&\mathbf{0}&\mathbf{0}\\-\boldsymbol{\Delta}_f^2&\mathbf{0}&-\boldsymbol{\Omega}_f^2&-\boldsymbol{\Delta}_f&\mathbf{0}&\mathbf{0}&\mathbf{0}&\mathbf{0}\\\mathbf{0}&\mathbf{0}&\mathbf{0}&\mathbf{0}&\mathbf{0}&\mathbf{I}&\mathbf{0}&\mathbf{0}\\\mathbf{0}&\hat{\mathbf{C}}_{pe}^{-1}\widehat{\boldsymbol{\theta}}_{pe}^T&\mathbf{0}&\mathbf{0}&-\hat{\mathbf{C}}_{pe}^{-1}\widehat{\boldsymbol{\Omega}}_s^2&-\hat{\mathbf{C}}_{pe}^{-1}\widehat{\boldsymbol{\Delta}}_s&\mathbf{0}&\mathbf{0}\\\mathbf{0}&\mathbf{0}&\mathbf{0}&\mathbf{0}&\widehat{\boldsymbol{\Delta}}_{sf}&\mathbf{0}&\mathbf{0}&\mathbf{I}\\\mathbf{0}&\mathbf{0}&\mathbf{0}&\mathbf{0}&-\widehat{\boldsymbol{\Delta}}_{sf}^2&\mathbf{0}&-\widehat{\boldsymbol{\Omega}}_{sf}^2&-\widehat{\boldsymbol{\Delta}}_{sf}\end{bmatrix}, \tag{36}$$

$$\mathbf{B}=\begin{bmatrix}\mathbf{0}&\left[\mathbf{M}_t^{-1}\boldsymbol{\Phi}_p\right]^T&\mathbf{0}&\mathbf{0}&\mathbf{0}&\mathbf{0}&\mathbf{0}&\mathbf{0}\end{bmatrix}^T\qquad\mathbf{C}_{\mathbf{q}}=[\mathbf{0}\quad\mathbf{I}\quad\mathbf{0}\quad\mathbf{0}\quad\mathbf{0}\quad\mathbf{0}\quad\mathbf{0}\quad\mathbf{0}] \tag{37,38}$$

$$\mathbf{C}_{\mathbf{q}f}=[\boldsymbol{\Delta}_f\quad\mathbf{0}\quad\mathbf{0}\quad\mathbf{I}\quad\mathbf{0}\quad\mathbf{0}\quad\mathbf{0}\quad\mathbf{0}]\quad\mathbf{C}_{\boldsymbol{\Lambda}f}=\begin{bmatrix}\mathbf{0}&\mathbf{0}&\mathbf{0}&\mathbf{0}&\widehat{\boldsymbol{\Delta}}_{sf}&\mathbf{0}&\mathbf{0}&\mathbf{I}\end{bmatrix}^T. \tag{39,40}$$

3.5 Time averaged energy functions

The optimisation study was carried out considering the filtered time averaged total flexural response of the panel and the filtered time averaged total power absorbed by the shunts given by [19]:

$$\bar{K}=E[K(t)]=E\left[\frac{1}{2}\dot{\mathbf{q}}_f^T\mathbf{M}_t\dot{\mathbf{q}}_f\right]=\frac{1}{4}\mathrm{Tr}\left[\mathbf{C}_{\mathbf{q}f}^T\mathbf{M}_t\mathbf{C}_{\mathbf{q}f}\mathbf{X}\right], \tag{41}$$

$$\bar{P}=E[P(t)]=E\left[\dot{\widehat{\boldsymbol{\Lambda}}}_{sf}^T\mathbf{C}_s^{-1}\mathbf{R}_s^{-1}\dot{\widehat{\boldsymbol{\Lambda}}}_{sf}\right]=\frac{1}{2}\mathrm{Tr}\left[\mathbf{C}_{\boldsymbol{\Lambda}f}^T\mathbf{C}_s^{-1}\mathbf{R}_s^{-1}\mathbf{C}_{\boldsymbol{\Lambda}f}\mathbf{X}\right], \tag{42}$$

where the covariance matrix $\mathbf{X}$ satisfies the Lyapunov equation

$$\mathbf{AX} + \mathbf{XA}^{\mathrm{T}} + \mathbf{BFB}^{\mathrm{T}} = \mathbf{0} \tag{43}$$

and $\mathbf{F} = E\left[\mathbf{f}_p \mathbf{f}_p^T\right]$ is the covariance matrix of the rain on the roof excitation, which in this study is assumed as an identity matrix.

3.6 Power spectral density of the time average kinetic energy

The effectiveness of the array of multi-resonant shunts was derived in terms of the spectrum of the plate total flexural kinetic energy Power Spectral Density (PSD), which is given by [26]:

$$S_K(\omega) = \tfrac{1}{2} m_p \mathrm{Tr}[\mathbf{M}_t \mathbf{Y}(\omega) \mathbf{S}_{\mathbf{ff}}(\omega) \mathbf{Y}^H(\omega)] \,, \tag{44}$$

where $\mathbf{S}_{\mathbf{ff}}(\omega)$ is the matrix with the PSD functions of the 16 uncorrelated white noise forces acting on the plate, which is therefore given by a 16×16 identity matrix. Also $\mathbf{Y}(\omega)$ is a matrix with self and cross modal mobility functions,

$$\mathbf{Y}(\omega) = \mathrm{j}\omega\left[-\omega^2 \mathbf{M}_t + \mathrm{j}\omega \mathbf{C}_p + \mathbf{K}_t + \mathrm{j}\omega \boldsymbol{\theta}_{pe} \mathbf{Z}_{spe} \boldsymbol{\theta}_{pe}^T\right]^{-1} \boldsymbol{\Phi}_p \,, \tag{45}$$

where $\mathbf{Z}_{spe} = \left[\mathbf{I} + \mathrm{j}\omega \mathbf{C}_{pe} \mathbf{Z}_s\right]^{-1} \mathbf{Z}_s$ and $\mathbf{Z}_s$ is a diagonal matrix with the multi-resonant impedances of the shunts, which were derived in Eq. (3).

4. Simulation results

As discussed in Ref. [12], the optimal RL parameters that should be implemented in a shunted piezoelectric patch to control the flexural response of a two dimensional flexible structure cannot be derived with closed form expressions. Therefore, the optimal shunt parameters that would reduce the low frequencies narrow band resonance peaks and mid frequencies wide band resonance crests, have been derived numerically considering the 10 bands in the spectrum of the kinetic energy PSD shown in Fig. 2, each of which encompass at least one resonance peak.

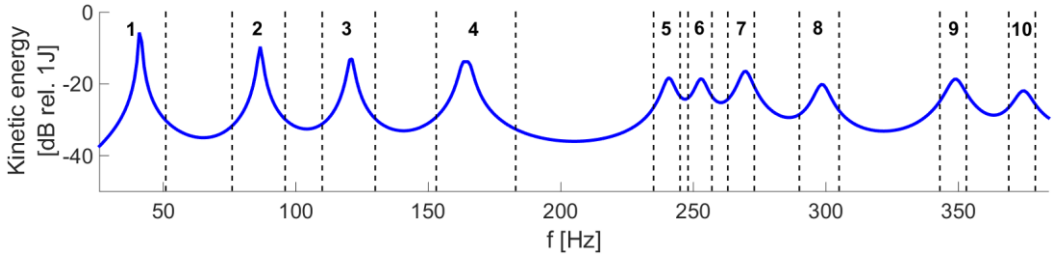

Figure 2: Flexural kinetic energy PSD of the plate and piezoelectric patches in open circuit configuration with highlighted the frequency bands considered in the shunts optimization study.

Plots A, D and B, E of Fig. 3 respectively present the panel flexural kinetic energy and the electric power absorbed by a RLC shunt averaged in the frequency bands 1 and 6 with respect to the resonance frequency f_s and quality factor Q_s of a simple RLC shunt. Thus, for example, plots A, D gives the optimal RLC values that should be implemented in the meshes of the multi-resonant shunts to minimise the resonant flexural response of the panel in the first and sixth frequency bands highlighted in Fig. 2. Contrasting plots A, D with the equivalent plots B, E, it is noted that the minimum of the filtered plate flexural kinetic energy and the maximum of the filtered electric power absorbed by the shunts occurs for very similar values of f_s and Q_s, that is for very similar values of the RLC components of the shunt. This is a rather interesting result, which indicates a practical approach to tune the multi-resonant shunts formed by a cascade of RLC meshes. Indeed, an iterative initialisation stage can be conceived where the RLC parameters of each mesh in the shunts are set to maximise the filtered electric power absorbed by the shunts. The spectra in plots C, F of Fig. 3, show the PSD of the panel flexural kinetic energy when the piezoelectric patches are either in open circuit (blue lines)

or connected to a RLC shunt that implements the optimal RLC values that minimise the panel flexural kinetic energy and thus maximise the power absorption of the RLC shunt. The plots also show the PSD of the electric power absorbed by the shunt (black line). The kinetic energy spectra show that, as one would expect with classical vibration absorbers, when the piezoelectric patches are connected to the optimal RLC shunts, the resonance peak that characterised the flexural response in the target band is split into two resonance peaks, which are effectively damped. As can be noted in the absorbed electric power spectrum, the energy subtracted to the structure to produce the damping effect is actually absorbed by the shunt. It is important to note that, as can be observed in Plots D and E of Fig. 3, for band 6, the optimal f_s of the shunts diverges from the resonant frequency of the plate within the analysed frequency band. This is due to the fact that, above about 200 Hz, the plate modal overlap exceeds unity and thus the response of the panel at each frequency is characterized by the superposition of an increasing number of higher order natural modes. Therefore the natural frequency of the optimal RLC shunt may diverge from the resonance frequency of the target resonance crest.

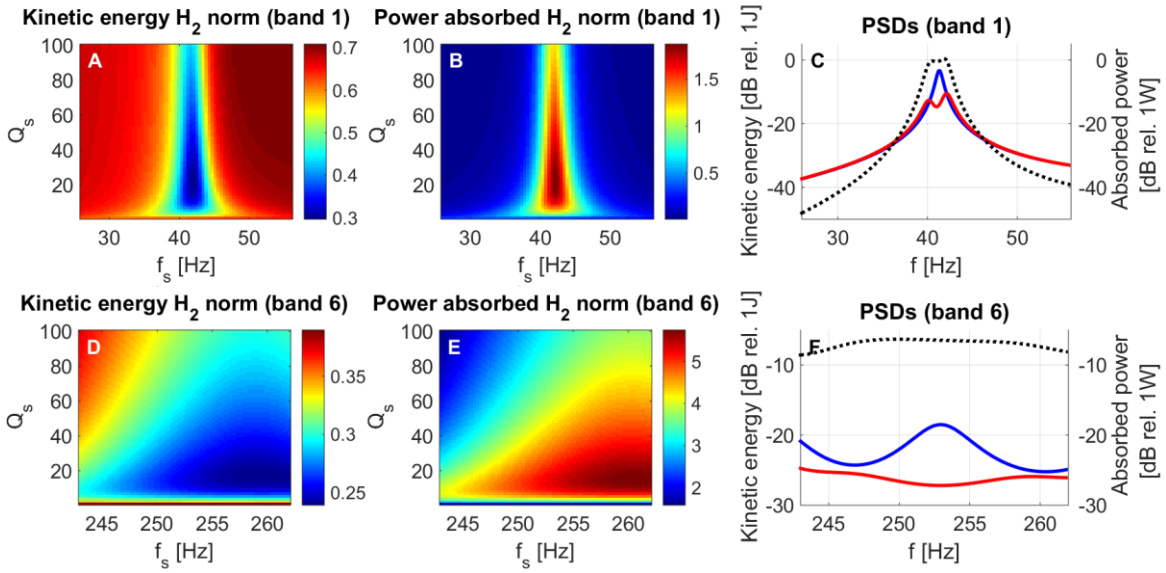

Figure 3: Flexural kinetic energy (Plots A, D) and power absorbed by a RLC shunt (Plots B, E) averaged in the frequency bands 1 and 6. Plots C, F, flexural kinetic energy PSD (open circuit blue lines; optimal RLC shunts red lines) and of the absorbed power PSD (optimal RLC shunts dotted black line).

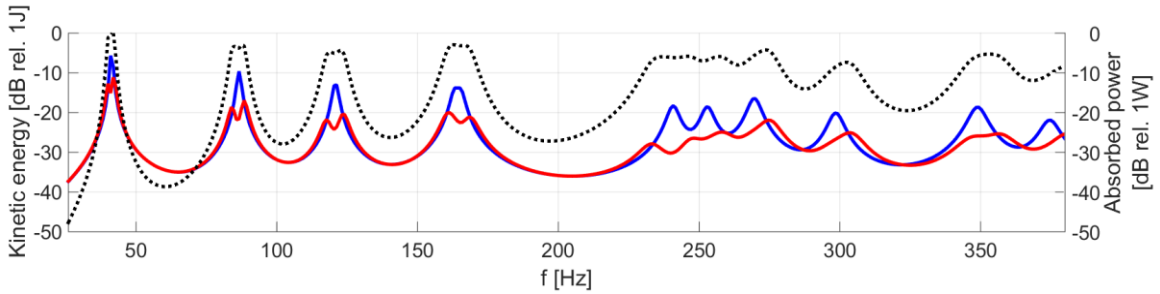

Figure 4: Kinetic energy PSD of the plate and piezoelectric patches in open circuit (blue line) and connected to idealised multi-resonant shunts (red), electric power absorbed by the shunts PSD (black line).

The optimal values of f_s and Q_s for the 10 frequency bands highlighted in Fig. 2 have been implemented into multi-resonant shunts formed by a sequence of then RLC meshes as shown in Fig. 1C. The plot in Figure 4 shows the 20 – 400 Hz spectra of the panel flexural kinetic energy PSD when the piezoelectric patches are either in open circuit (blue lines) or connected to the multi-resonant meshes whose RLC components were derived in such a way to maximise the electric power absorbed by RLC shunts in the 10 frequency bands highlighted in Figure 2. The plot also shows the PSD of the electric power absorbed by the shunt (black line). The graph confirm that the array of piezoelectric

patches with multi-resonant shunts produces a significant reduction of the flexural response of the panel in the whole 20 – 400 Hz frequency band. The low frequency sharp resonance peaks are lowered by 5 to 10 dB; but also the higher frequency wide band crests are brought down by about 6 to 10 dB.

5. Conclusions

This paper has presented a simulation study on the implementation of a dense array of piezoelectric patches connected to multi-resonant shunts formed by a cascade of RLC meshes. The RLC meshes were tuned in such a way as to minimise the flexural kinetic energy of the panel averaged in target frequency bands. The study has shown that this control strategy is equivalent to the maximisation of the electric power absorbed by the shunts, which is a more practical cost function to be implemented. Finally, the study has shown that when the multi-resonant shunts are implemented with a cascade of 10 RLC meshes tuned to maximise the electric power absorbed by the shunts in 10 target frequency bands, the flexural response of the panel in the 20 to 400 Hz band is reduced by 5 to 10 dB.

ACKNOWLEDGMENTS

The authors gratefully acknowledge the European Commission for its support of the Marie Skłodowska-Curie program through the ITN ANTARES project (GA 606817).

REFERENCES

1 D.J. Mead *Passive Vibration Control* John Wiley & Sons (1999).
2 Z. Liu, X. Zhang, Y. Mao, Y. Y. Zhu, Z. Yang, C. T. Chan, P. Sheng, Locally resonant sonic materials. *Science*, **289** (5485), 1734-1736, (2000).
3 R. L. Forward, Electronic damping of vibrations in optical structures, *Applied Optics*, **18**(5) 690-697, (1979)
4 G. A. Lesieutre, Vibration damping and control using shunted piezoelectric materials, *The Shock and Vibration Digest*, **30** (3), 187-195.
5 M. Ahmadian, P. DeGuilio, Recent advances in the use of piezoceramics for vibration suppression, *The shock and Vibration Digest*, **33** (1), 15-22, (2001).
6 S. O. R. Moheimani, A survey of recent innovations in vibration damping and control using shunted piezoelectric transducers, *IEEE Transactions on Control Systems Technology*, **11** (4), 482-494, (2003).
7 S. Moheimani, A. Fleming, *Piezoelectric transducers for vibration control and damping*, Springer (2006)
8 F. Casadei, M. Ruzzene, L. Dozio, K. A. Cunefare, Broadband vibration control through periodic arrays of resonant shunts: experimental investigation on plates, *Smart Materials and Structures*, **19** (1), (2010).
9 S. Alessandroni, U. Andreaus, F. dell'Isola, M. Porfiri, Piezo-ElectroMechanical (PEM) Kirchhooff-Love plates, *European Journal of Mechanics A/Solids 23*, (2004).
10 L Airoldi, M. Ruzzene, Design of tunable acoustic metamaterials through periodic arrays of resonant shunted piezos, *New Journal of Physics* **13**, (2011).
11 B. Lossouarn, J-F. Deu, M. Aucejo, K. A. Cunefare, Multimodal vibration damping of a plate by piezoelectric coupling to its analogous electrical network, *Smart Materials and Structures*, **25** (11), (2016).
12 P. Gardonio and D. Casagrande, Shunted piezoelectric patch vibration absorber on two-dimensional thin structures: Tuning considerations, *Journal of Sound and Vibration*, **395**, 26-47, (2017).
13 D. Casagrande P. Gardonio, M. Zilletti, Smart panel with time-varying shunted piezoelectric patch absorbers for broadband vibration control, In press *Journal of Sound and Vibration*, (2017).
14 J.N. Reddy, *Mechanics of Laminated Composite Plates and Shells: Theory and Analysis*, CRC Press, (2004)
15 N.W. Hagood, W.H. Chung, A. von Flotow, Modelling of piezoelectric actuator dynamics for active structural control *Journal of Intelligent Material Systems and Structures* **1**, 327-354, (1990).
16 A. Preumont, *Mechatronics*, Springer, Dordrecht, (2006).
17 S.H. Crandall, D.C. Karnopp, A.F. Kurtz, D.C. Pridmore-Brown, *Dynamics of Mechanical and Electromechanical Systems*, R. E. Krieger Pub. Co., Malabar, Florida, (1982).
18 L. Meirovitch, *Principles and Techniques of Vibration*, Prentice Hall, Upper Saddle River, NJ, (1997).
19 P. Gardonio, S. Miani, F. Blanchini, D. Casagrande and S.J. Elliott, Plate with decentralised velocity feedback loops: Power absorption and kinetic energy considerations, *J. of Sound and Vib.* **331** 1722-1741, (2012)